Catalysis Science & Technology

Relationship between ZSM-5 pore modifications and gallium proximity and liquid hydrocarbon number distribution from ethanol oligomerization

Journal:	*Catalysis Science & Technology*
Manuscript ID	CY-ART-02-2022-000288.R1
Article Type:	Paper
Date Submitted by the Author:	01-Jun-2022
Complete List of Authors:	Seemala, Bhogeswararao; University of California Riverside, CE-CERT Wyman, Charles; UCR, Chemical and Environmental Engineering

Relationship between ZSM-5 pore modifications and gallium proximity and liquid hydrocarbon number distribution from ethanol oligomerization

Bhogeswararao Seemala[1,*], Charles E Wyman[1,2]

[1]Center for Environmental Research Technology, Bourns College of Engineering, University of California Riverside, Riverside, California, 92507, USA.
[2]Department of Chemical and Environmental Engineering, Bourns College of Engineering, University of California Riverside, Riverside, California, 92507, USA.

***Corresponding Author email: bhogeshwar.rao@gmail.com or bseemala@engr.ucr.edu**

Abstract

Jet fuel from petroleum provides energy densities and other attributes vital for aviation but adds to greenhouse gas emissions. Biomass provides an inexpensive resource that is uniquely suited for large-scale conversion into low carbon footprint sustainable aviation fuels (SAF) for the immediate future and likely longer. Through a pool mechanism, novel consolidated alcohol deoxygenation and oligomerization (CADO) ZSM-5 catalysts offer low-cost, one-step, complete conversion of biomass ethanol into hydrocarbons without adding hydrogen. However, CADO products mostly contain less than 8 carbon atoms while jet fuel includes up to 16, likely restricting jet fuel blending to 50% or less. To overcome this limitation, the effectiveness of reacting ZSM-5 with 0.2, 0.6, 0.8, and 1.0M sodium hydroxide concentrations over a range of temperatures and times was evaluated for enhancing the carbon number range. X-ray diffraction, N_2-physisorption, X-ray photoelectron spectroscopy, H_2-TPR, and STEM showed that treating with 0.8M sodium hydroxide at 60°C for 0.5hour increased pore volumes and metal-support interactions more than lower concentrations while retaining crystallinity better than for 1.0M treatment. The larger pores enhanced 5wt.% gallium oxide migration into ZSM-$5_{0.8M}$ channels and promoted strong interactions between gallium oxide and the support that coupled with retained crystallinity and greater capacity for larger molecules increased liquid hydrocarbon yields (LHYs) from pure ethanol to 46.1% and C9-

C10 aromatics selectivity to 45.8%, the first reported direct increase in C9-C10 aromatics selectivity from ethanol. In addition, cofeeding 60% water with ethanol further enhanced LHY and C9-C10 aromatics selectivity to 53.1% and 55.1%, respectively, while extending catalyst stability.

Introduction

Transportation contributes 36% of total US 2020 carbon dioxide emissions, a greater amount than from any other US end use sector, and powering transportation by petroleum derived fuels accounts for 97% of these emissions (EIA report).[1,2] The primary focus to power light duty vehicles is now to phase in electric batteries and fuel cells, albeit carbon emissions will continue during the considerable time needed to displace current fleets and fuels. However, if aviation is to meet its important carbon emission reduction targets higher mass energy densities are needed than currently possible by electric power.[3] On the other hand, biomass conversion to liquid fuels provides the lowest cost option for production of sustainable aviation fuels (SAF) with properties comparable to those for jet fuel derived from petroleum.[4–7] The challenge is that conventional jet fuel is a complex mixture that generally consists of 75-85 vol% iso-paraffins and cyclo-paraffins with the rest being aromatics to swell seals and meet other fit-for-purpose requirements. A recent IEA report outlined technologies and projected costs for most sustainable options under current investigation for production of SAF that could replicate key properties needed for jet fuel.[8] In this study, hydroprocessed esters and fatty acid (HEFA) fuels were shown to currently provide the largest amount of fuel at a reasonable cost, but limited supplies of low-cost plant oils could impede substantial growth. Other options such as catalytic conversion of syngas to SAF could also play a role. A particularly promising route that could facilitate rapid transformation to low carbon emissions by aviation is catalytic conversion of ethanol into SAF that meets energy density and other fit-for-purpose requirements and can build on established US and world ethanol production of about 14 and 26 billion gallons, respectively, by far the largest amount of biofuel in 2020.[4,9]

Many of these alcohol to jet (ATJ) processes being scaled up require 3 to 4 catalytic steps to dehydrate ethanol to C2 to C4 olefins, oligomerize these olefins to C6 to C8 products, further polymerize the oligomers to higher carbon number compounds, and saturate double bonds by hydrogenation. In addition to entailing multiple steps, these operations require high temperatures and pressures and can suffer from compounding of the yield losses of each step. On the other hand, a new consolidated alcohol deoxygenation and oligomerization (CADO) technology employs zeolite catalysts to combine ethanol dehydration/deoxygenation, oligomerization, and further reaction in a single step without the need to add hydrogen. However, although the high aromatic content and carbon number distribution from CADO are currently suitable for high level blending with gasoline, shifting the product distribution to higher carbon number compounds would increase blend levels for jet fuel. Hence, this study focuses on determining how changes in ZSM-5 zeolite catalyst features can increase the carbon number range of liquid hydrocarbons made from ethanol by CADO technology and thereby allow higher blend levels in aviation fuels.

Si/Al ratio, crystal size, weight hour space velocity(WHSV), temperature, and reaction pressure have been optimized for ethanol conversion into hydrocarbons using H-ZSM-5 supports.[10–13] When ethanol is co-fed with inert gases and reaction pressures are maintained above 20 bar for such catalysts, gasoline range paraffins and benzene/toluene/xylene (BTX) are more predominant products while ethylene is the dominant product for reactions at atmospheric pressure without an inert gas carrier.[14–18] The effect of loading various metals on H-ZSM-5 supports have also been extensively studied for BTX production from ethanol. For example, Inaba et al. reported selectivity for BTX production from ethanol dropped in the order Ga >> Pd > Ir > Au > Ru > Rh > H-ZSM-5 for reaction at 400°C and 0.1589 WHSV for a nitrogen flow rate of 60 cm^3/min.[19] In another study, Ga doped ZSM-5 catalyst had better stability than Zn doped ZSM-5 for ethanol

conversion to BTX at 360°C and $1h^{-1}$ WHSV.[20] Van der Borght et al. highlighted the importance of low Ga metal (<1%) loadings onto ZSM-5 to prevent pore blocking and provide maximum access for reactants to interact with acid sites to produce BTX.[21] A detailed study by Li et al. demonstrated loading 6.2% gallium oxide on ZSM-5 promoted BTX selectivity while producing ≤ 7% C8+ aromatics at 450°C and $0.4h^{-1}$ WHSV.[22] Interestingly, gas chromatographic analysis of filtrate recovered by washing of post-reaction/used H-ZSM-5 catalyst with dichloromethane solvent showed C9-C14 aromatics had been formed.[23] Based on this result, they hypothesized that an ethanol dual-cycle hydrocarbon pool (HCP) mechanism progressively formed C9+ aromatics in addition to BTX. However, because these molecules are larger than the H-ZSM-5 pores, i.e., 4.5 × 5.2A˚ for straight pores with an internal pore space of 6.19A˚, the large substituted aromatic molecules produced had to crack to smaller BTX molecules to escape from the micropores as otherwise they would block ZSM-5 acidic sites in the framework.[23–25] On the overhand, the HCP process was not favored for ethanol conversion over larger micropore zeolites such as H-Beta, USY, and H-mordenite, with the result that BTX production was low and heavy coking resulted.[19]

The above studies clearly highlighted that H-ZSM-5 supports selectively produce BTX by the ethanol HCP process and Ga addition to H-ZSM-5 further promoted BTX production (C6-C8 aromatics only). However, in these studies, most of the gallium oxide was proven to be on the external zeolite surface due to steric constraints to incorporation inside the pores.[19–23,26–29] Although it is still unclear what role gallium oxide inside the zeolite channels plays on ethanol product distributions, some reports mentioned that the small fraction of Ga located in H-ZSM-5 channels enhanced BTX selectivity.

To address this issue, we hypothesized that increasing H-ZSM-5 pore volumes by post synthesis would facilitate greater gallium insertion into the zeolite channels. Furthermore, it was

reasoned that enhanced zeolite pore volumes inside zeolite pores would accommodate longer hydrocarbon chain lengths that are desirable for jet fuel. To test this concept, a simple, efficient, and reproducible desilication process that is selective for extracting framework silica without disturbing framework alumina/Bronsted acid sites and for creating new mesopores was adopted for H-ZSM-5 (Si/Al – 23).[30–34] In particular, H-ZSM-5 (Si/Al-23) supports were desilicated by treatment with NaOH to produce mesopore-crystalline H-ZSM-5. Then, Ga was loaded onto parent and modified ZSM-5 supports by following incipient wet-impregnation procedures, and the resulting catalysts were used to catalyze ethanol conversions at different temperatures and WHSVs. The effects of Ga proximity on the zeolite external surface and inside the channels on ethanol product distributions were then determined.

Experimental

Materials:

ZSM-5 (Product code: CBV 2314, Zeolyst International, Kansas City, Kansas), NaOH (99.99%, Fisher Chemicals, Hampton, NH), ammonium nitrate (99.99%, Spectrum Chemicals MFG Corporation, Gardena, CA), and ethyl alcohol (99.5%, Spectrum Chemicals MFG Corporation, Gardena, CA) were employed for these studies.

Catalyst synthesis:

Desilication of H-ZSM-5: Framework silica was extracted/removed from H-ZSM-5 supports by treatment with 0.2M, 0.6M, 0.8M, and 1.0M NaOH solutions to synthesize ZSM-$5_{0.2M}$, ZSM-$5_{0.6M}$, ZSM-$5_{0.8M}$ and ZSM-$5_{1.0M}$, respectively. These modified supports are hereafter referred to as ZSM-5_{xM}, in which x indicates the Molarity. First, the appropriate amount of ZSM-5 was mixed with aqueous NaOH solution at 60°C by magnetic stirring for 0.5hours (IKA® C-MAG HS, 7, Sigma-Aldrich, Inc., St. Louis, MO). The reaction mixture was quickly quenched in

an ice water bath and centrifuged (Beckman Coulter®, Brea, CA) to separate and wash the solids with deionized-water until the filtrate pH reached 7. The desilicated solids were then dried in an oven (Heratherm Oven, Thermo Scientific, Waltham, MA) at 105°C for 6 hours.

Ammonium nitrate treatment: To regenerate the protonic form of zeolites from each Na-ZSM-5_{xM}, 2g of the desilicated solids were added to 120ml of deionized water containing 3.298g of aqueous ammonium nitrate, and the resulting mixture was heated at 80°C while magnetically stirring for 24 hours (IKA® C-MAG HS, 7, Sigma-Aldrich, Inc., St. Louis, MO). During this time, decomposition of the ammonium nitrate released ammonia and protons, with the latter replacing Na^+ ions in Na-ZSM-5. Next, the solids were separated from the liquid by centrifugation (Beckman Coulter®, Brea, CA) and dried at 105°C for 6 hours (Heratherm Oven, Thermo Scientific, Waltham, MA) followed by calcining at 500°C for 5 hours (Model 120, Fisher Scientific, Waltham, MA).

Ga/ZSM-5 catalysts synthesis: For this study, 5 wt.% Ga was loaded onto ZSM-5 and each ZSM-5_{xM} by following the incipient wet-impregnation procedure. In a typical synthesis, the appropriate amount of gallium nitrate precursor was dissolved in water and then added to H-ZSM-5 or ZSM-5_{xM} at a water/ZSM-5 mass ratio of 50:1. This combination was then mixed on a magnetic hot-plate (IKA® C-MAG HS, 7, Sigma-Aldrich, Inc., St. Louis, MO) that also kept the temperature at 80°C for 16 hours for most samples. However, a few samples were wet-impregnated for 4 hours and 32 hours. The solid material was separated from the liquid using a rotary evaporator (Model-RE-501, Lanphan Technology Co. Ltd, Zhengzhou, Henan, China). The solid obtained was dried at 105°C for 6 hours and calcined at 500°C for 5 hours by a muffle furnace (Model 120, Fisher Scientific, Waltham, MA) at a ramp rate of 10°C/min from 25°C. A similar procedure was followed for 2 wt.% and 8 wt.% Ga impregnations on the ZSM-$5_{0.8M}$ support. Without any further

pretreatment, as-synthesized materials were used for catalytic conversion of ethanol at 350°C, 400°C, 450°C, and 500 °C and space velocities of 1.6, 1.2, 0.8, and 0.4h^{-1}, unless otherwise noted.

Catalyst characterization:

X-ray diffraction (XRD): XRD spectra of all gallium loaded catalysts were recorded in the 2θ range of 20 to 90° using an X'pert Pro PANalytical diffractometer (Malvern PANalytical, Empyrean Series 2, Westborough, MA), equipped with a Nickel filtered Cu-Kα radiation source.

Surface Area: The total accessible surface area (S_{BET}) and pore volume of the catalysts were measured by N_2 physisorption using a Micromeritics (Micromeritics, ASAP 2020, Norcross, GA) instrument. The mesopore volume and size distribution were estimated from the desorption branch of the isotherm by applying the Barrett−Joyner−Halenda (BJH) model.

Inductively Coupled Plasma-Optical Emission Spectroscopy (ICP-OES): Metal concentrations in the solids were measured by ICP-OES analysis using a Perkin-Elmer Optima (7300DV, Thermo Fisher, Richmond, CA) ICP-OES apparatus that combines an SCD detector and an echelle optical system.

Scanning Transmission Electron Microscopy (STEM): STEM imaging was at 300 kV accelerating voltage on a FEI/Philips (Titan Themis 300, ThermoFisher Scientific, Hillsboro, OR) Titan Themis 300 instrument fitted with an X-FEG electron source, a three-lens condenser system, and an S-Twin objective lens. STEM images were recorded with a M3000 High Angle Annular Dark Field (HAADF) Detector (Fischione Instruments Inc., Export, PA) at a probe current of 0.2 nA, frame size of 2048 × 2048, dwell time of 15 μs/pixel, camera length of 195 mm, and convergence angle of 10 mrad. Elemental X-ray microanalysis and mapping utilized a FEI Super-X EDS system with four symmetrically positioned SDD detectors of 30 mm^2 each, resulting in an effective collection angle of 0.7 srad. Elemental maps were collected in STEM mode with a beam

current of 0.4 to 0.25 nA, a 512 × 512-pixel frame, 30 μs dwell time, and up to 10 min acquisition time. Specimens prepared from suspensions in distilled water were deposited on copper grids coated with lacey carbon (300 mesh Cu, Ted Pella Inc, Redding, CA). Average metal particle sizes were measured based on the diameter of 100 particles from corresponding TEM images of each catalyst.

X-ray photoelectron spectroscopy (XPS): XPS characterization was by a Kratos XPS system (AXIS ULTRADLD, Shimadzu, Chestnut Ridge, NY) equipped with an Al Kα monochromated X-ray source and a 165-mm mean radius electron energy hemispherical analyzer. Vacuum pressure was kept below 3×10^{-9} torr during analysis. Binding energy calibrations were with reference to the carbon 1s peak by adjusting spectra to 284.8 eV. Surface composition of gallium was calculated using sensitivity factors of 5.581.

H_2-Temperature Program Reduction and Oxidation studies: H_2-Temperature program reduction (TPR) and temperature program oxidation (TPO) experiments were conducted with a Hiden Analytical CATLAB instrument (2375 Maxwell Lane, Sedona, AZ 86336). For H_2-TPR experiments, a 100mg sample was dried in a 2% O_2/He stream for 1 h at 450°C and then cooled to 150 °C prior to analysis. Then the sample was reduced in a 10% H_2/He (50 mL/min) stream at a heating rate of 10°C/min to 950°C. TPO characterization techniques were applied in the same system to about 100mg of catalysts that had been used for ethanol and wet-ethanol streams. Prior to analysis, the samples were dried in a 2% O_2/He stream (30 mL/min) at 150°C for 1 h, followed by heating at a ramp up rate of 10°C/min to 950°C. Peaks for CO_2 (m/z = 44), CO (m/z = 28), and H_2O (m/z = 18) were recorded with a mass spectrometer (Hiden Quadrupole, 2375 Maxwell Lane, Sedona, AZ 86336).

Reactivity experiments:

Liquid product analysis: Organic liquid products were analyzed using an Agilent Technologies 7890A gas chromatograph (7890 A, Agilent Technology, Santa Clara, CA) equipped with a 30 m long × 0.320 mm internal diameter × 20 micron HP-PLOT/Q-column and an FID detector (Agilent Technology, Santa Clara, CA). The GC program held the column at 50°C for 3 min followed by ramping from 50 to 250°C at 15°C min^{-1} and then holding at 250°C for 50 min. Product concentrations were quantified based on calibration curves of standard samples measured following the same protocol on the same equipment. Ethanol conversion, theoretical liquid hydrocarbon yields (THY), liquid hydrocarbon yields (LHY), and product selectivity were calculated as follows:

Equation 1: Ethanol conversion = $1 - \frac{Moles\ of\ unreacted\ ethanol}{Moles\ of\ ethanol\ before\ reaction}$

Percent liquid product selectivity (LPS) to form hydrocarbons of chain length C: LS $= \frac{Mass\ of\ C\ compound\ collected}{Total\ mass\ of\ organic\ liquid\ collected}\ X\ 100$

Liquid hydrocarbon yields (LHYs) = $\frac{\text{Mass of liquid HC in product (g)}}{Theoretical\ HC\ yield\ from\ ethanol\ (g)}$

Theoretical liquid HC yield = $Mass\ of\ ethanol\ feed\ (g)\ X\ 0.564$

Catalyst performance evaluations: Ethanol catalytic reactions were run with a custom-made stainless steel fixed-bed reactor (1/4" diameter by 6.5" inch long stainless-steel tube) fed ethanol through a heated line into the catalytic reactor. Temperatures in the preheating line and reactor bed were monitored by a PID controller, and liquid hydrocarbon products from the reactor were condensed for collection by cooling the outlet line to below 5°C. For each reactor run, a high precision peristaltic pump (DRIVE MFLEX L/S 100RPM 115/230 Cole-Parmer, IL) controlled ethanol inlet flows at desired rates through 0.6 g of as-synthesized Ga-ZSM-5 or Ga-ZSM-5_{xM}

catalyst powder. The catalyst was preheated to 500°C for 1 hour at an ethanol space time velocity of $1.6h^{-1}$ prior to heating up to 350, 400, 450, or 500 °C for the catalyst performance evaluations. After running at steady-state for 3 hours, liquid products were collected every two hours from the reactor outlet. The products usually contained liquid and gaseous hydrocarbons plus a significant amount of water (theoretically 39.07 g of water from 100 g of ethanol) with little ethanol left. Because water would quickly damage the gas chromatograph (GC) packing, liquid hydrocarbons were extracted from the water with dichloromethane before injecting into the GC for liquid hydrocarbon analysis. Hydrocarbon gases were not analyzed to avoid GC column damage by vaporized water. Reported catalyst performance data were based on analyses of the organic liquid product collected after at least 4 hours of reactor operation. Catalyst performance and stability were determined for feeding either pure ethanol or 40% ethanol in water for 32 hours. Used catalyst recovered after reaction was washed with dichloromethane to remove organic deposits and then calcined prior to characterization by XRD, N_2-physisorption, and XPS.

Results and Discussion

*Effect of NaOH treatment on catalyst characteristics***:**

To understand what caused differences in ethanol oligomerization and product distribution from ethanol reactions on the different treated ZSM-5 supports, crystallinity, pore volume, gallium oxide particle size, binding energy, and surface Si/Ga ratio of all synthesized catalysts were determined by XRD, S_{BET}, STEM, and XPS techniques.

Figure 1a pictures X-ray diffraction (XRD) patterns of H-ZSM-5 and alkali treated H-ZSM-5_{xM} catalysts. As shown, typical ZSM-5 diffraction peaks identified in the 2θ range of 22.8 to 25.0 are consistent with those for reference ZSM-5 (PDF#44-0003). However, the shape and intensity of diffraction peaks for alkali treated ZSM-5_{xM} catalysts were altered due to extraction of

framework silica. Minimal losses in the intensity of ZSM-5 characteristic reflections were observed after treating ZSM-5 with 0.2, 0.6 and 0.8M NaOH, but 1.0M NaOH treatment resulted in significant loss of both diffraction peak shape and intensity. As reported in Table 1, the larger amount of NaOH could damage framework silica and potentially hurt ZSM-5 crystallinity. The relative crystallinity of these materials calculated from the signal area in the 22.7° to 24.2° range decreased in the following order: ZSM-5(100%) > ZSM-$5_{0.2M}$ (94.7%) > ZSM-$5_{0.6M}$ (90.3%) > ZSM-$5_{0.8M}$ (82.4%) > ZSM-$5_{1.0M}$(72.9%). As shown in Table S1, removing framework silica as measured from ICP-OES experiments resulted in a gradual loss in crystallinity. Thus, treating ZSM-5 with 1.0M NaOH suddenly increased both silica and alumina losses to nearly 40% of the total material (Table S1). X-rays did not show any gallium oxide peaks, suggesting gallium oxide was amorphous. But the shift in XRD peaks to higher angles for the alkali treated H-ZSM-5 might increase ZSM-5 unit-cell dimensions.

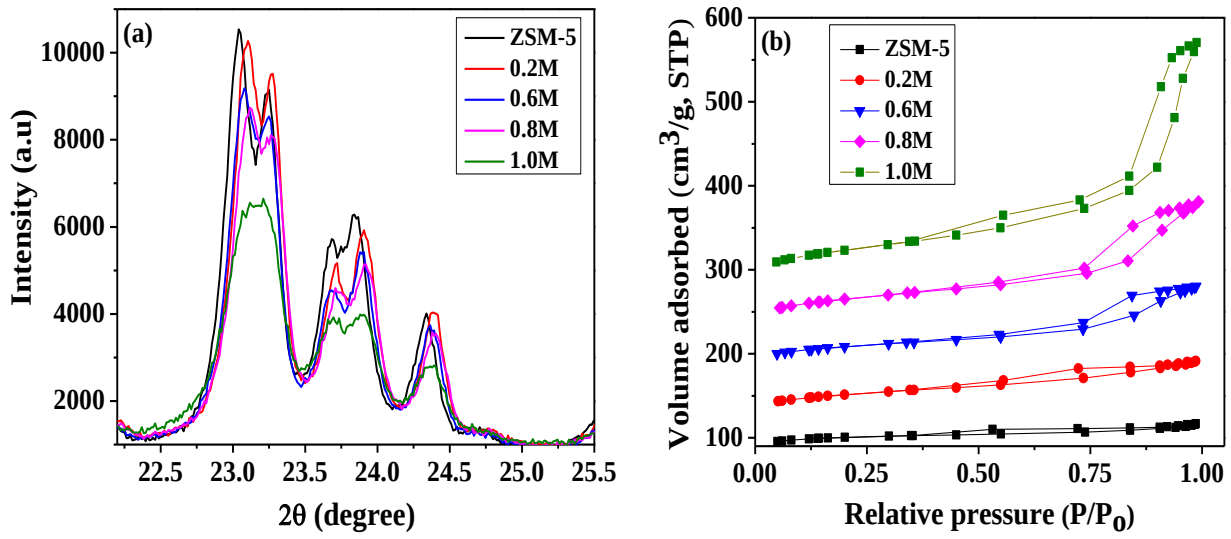

Figure 1: Effect of NaOH treatment concentration on (a) X-ray diffraction spectra and crystallinity and (b) N_2 adsorption-desorption isotherms for Ga(5 wt.%)/ZSM-5 and Ga(5 wt.%)/modified-ZSM-5 catalysts.

Figure 1b shows N_2 adsorption-desorption isotherms for Ga(5 wt.%)/ZSM-5 and Ga(5 wt.%)/ZSM-5_{xM} catalysts, and the corresponding BET total surface areas (SA), external surface areas, and mesopore volumes reported in Table 1. As shown, Ga/ZSM-5 exhibited a type-I isotherm and no distinct hysteresis loop, indicating a typical micro-porous structure even after Ga incorporation. Upon alkali treatment with NaOH, all Ga/ZSM-5_{xM} catalysts except Ga/ZSM-$5_{0.2M}$ took up more N_2 and displayed a type-4 isotherm with a H4-hysteresis loop, indicating enhanced total surface area and mesopores formation (Table 1 & Figure S1). Furthermore, the enhanced total and external surface areas in modified-ZSM-5 supports was due to newly formed pore walls and more outer surface area of microcrystallites.[35] However, 0.2M alkali treatment of ZSM-5 had little effect on both total SA and mesopore volume, suggesting minimal removal of framework silica, removed framework silica on the external framework, or blocking of micropores. On the other hand, Table 1 shows mesopore volumes increased by 1.5, 2.6, and 4 times when ZSM-5 was treated with 0.6M, 0.8M, and 1.0M NaOH, respectively. Although 1.0M NaOH treatment of ZSM-5 resulted in significant improvements in mesopore volume, excessive silica removal from the framework significantly damaged ZSM-$5_{1.0M}$ crystallinity, as shown by XRD results. The BJH pore size distribution curves in Figure S1 showed H-ZSM-5 mesopore size consistently increased with increasing NaOH concentration.

Table 1: Physicochemical properties of Ga(5 wt.%)/ZSM-5 and Ga(5 wt.%)/modified-ZSM-5 catalysts.

Catalyst	XRD,	N_2-adsorption-desorption			XPS,
	Relative crystallinity of support	Total Surface Area (SA; m^2/g)	External Surface Area (ESA; m^2/g)	Meso and Macro Pore Volume (cm^3/g)	External Surface ratio of Si/Ga
Ga(5%)/ZSM-5	100	338	60.1	0.064	5.4
Ga(5%)/ZSM-$5_{0.2M}$	94.7	334	64.6	0.092	6
Ga(5%)/ZSM-$5_{0.6M}$	90.3	366	106.7	0.156	14
Ga(5%)/ZSM-$5_{0.8M}$	82.4	393	134.2	0.238	13.5
Ga(5%)/ZSM-$5_{1.0M}$	72.9	421	170.6	0.457	12.5

STEM images of Ga(5 wt.%)/ZSM-5 and Ga(5 wt.%)/ZSM-$5_{0.8M}$ catalysts in Figures 2 and S3 show both contained large needle shaped gallium oxide particles with sizes of 0.5-1.5μm and 0.25-0.8μm, respectively. Figure S4s also indicates gallium oxide nanoparticles had an average diameter of 4.1±1.3nm and 3.8±1.8nm on parent-ZSM-5 and ZSM-$5_{0.8M}$ supports, respectively, consistent with a previous report.[36] Alkali treatment of ZSM-5 marginally increased the number of gallium oxide nanoparticles and gallium oxide dispersion by reducing the size of micro size gallium oxide particles on the external ZSM-$5_{0.8M}$ support. STEM images of the ZSM-$5_{0.8M}$ support in Figures 2 and S3 clearly suggest that NaOH treatment selectively extracted silica from the zeolite crystals and facilitated mesopores formation. Generally, the negatively charged framework tetrahedral alumina zeolite species as determined by ICP-OES and recorded in Table S1 are inert under NaOH treatment.[34]

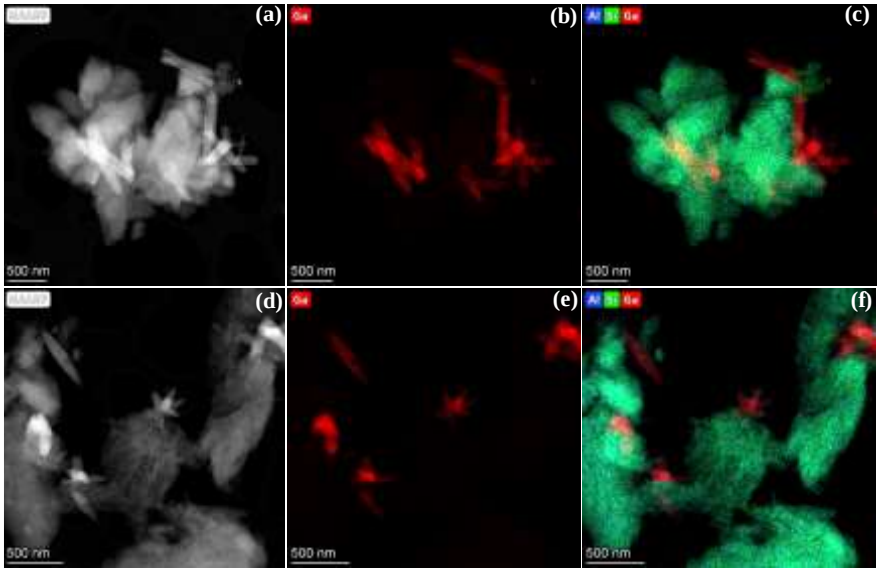

Figure 2: (a) STEM images of Ga(5 wt.%)/ZSM-5, (b) Ga, and (c) overlaid Ga/Si/Al elemental mapping. STEM images of (d) Ga(5 wt.%)/ZSM-$5_{0.8M}$, (e) Ga, and (f) overlaid Ga/Si/Al elemental mapping.

XPS spectra were collected for Ga(5 wt.%)/ZSM-5 and Ga(5 wt.%)/ZSM-5_{xM} catalysts to determine Ga binding energy (B.E) and surface Si/Ga ratios. Figure 3 shows Ga 2p3/2 XPS spectra of as-synthesized catalysts, and Table S3 lists surface Si/Ga ratios. Generally, the higher Ga 2p3/2 peak B.E for supported Ga_2O_3 catalysts in the 1117.8 to 1118.5eV range than for bare Ga_2O_3 particles could result in either strong metal-support interactions or Ga^{+3} bounded to neighboring oxygen or strong interactions of gallium $(GaO)^+$ with zeolite framework.[37–41] But in the present study, the Ga 2p3/2 peak B.E observed at 1118.8eV for all catalyst cases indicated Ga to be in as native oxide that formed a thin oxide layer on the outer surface.[42]

Figure S5 shows that applying 2 and 8% gallium loadings for 4 hours and 32 hours Ga wet-impregnation synthesis times had no effect on the B.E of Ga 2p3/2 peak, thereby indicating similar Ga electronic structures for all cases. The surface Si/Ga ratio for all catalysts were calculated from Ga, Si, Al and O metal XPS peak areas and normalized by their relative sensitivity factors (see Table 1 and S3). Interestingly, surface Si/Ga ratios nearly doubled for Ga/ZSM-$5_{0.6,0.8\&1.0M}$

catalysts compared to Ga/ZSM-5 and Ga/ZSM-$5_{0.2M}$ due to decreased Ga on the surface. In other words, enhancing pore volume of modified-ZSM-5 supports by treating with higher NaOH concentrations promoted greater Ga migration into the zeolite channels[38]. Reducing the Ga loading to 2% on ZSM-$5_{0.8M}$ increased the surface Si/Ga ratio to 29, while increasing the Ga loading to 8% resulted in a Si/Ga ratio 13, nearly the same as when 5 wt.% Ga was loaded onto ZSM-$5_{0.8M}$.

H_2-TPR was applied to determine the gallium oxide reduction temperature, nature of the gallium oxide, and metal-support interactions. The broad span of H_2-TPR reduction peaks from 500°C to 950°C for Ga(5 wt.%)/ZSM-5 and Ga(5 wt.%)/ZSM-5_{xM} catalysts shown in Figure S6 suggest that gallium oxide took different forms, consistent with our STEM data and previous reports.[43,44,45,46] Generally, gallium oxide nanoparticles are known to be reduced at 500°C to 600°C (external surface small Ga_2O_3 particles reduce to Ga^+), whereas the GaO^+ ions and surface segregated large gallium oxide clusters (extra framework (EF)-Ga_2O_3; 200nm to 1500 nm) are reported to be reduced at above 650°C and 800°C, respectively.[46] In the present case of Ga (5 wt.%)/ZSM-5, gallium oxide reduction began at 504°C, whereas gallium oxide reduction for modified support cases started in the following order as temperature was increased: Ga(5 wt.%)/ZSM-$5_{0.2M}$ (543°C) < Ga(5 wt.%)/ZSM-$5_{0.6M}$ (550°C) < Ga(5 wt.%)/ZSM-$5_{0.8M}$ (560°C). These results clearly suggested that more severe zeolite modifications enhanced metal-support interactions between gallium oxide and the ZSM-5 support.

As the nature of the gallium oxide plays an important role in ethanol oligomerization/aromatization, H_2-TPR profiles of 2, 5, and 8 wt% Ga loadings on ZSM-5, modified-ZSM-5 catalysts, and Ga loaded beta and Y-zeolite catalysts were deconvoluted and the data compared, as shown in Figures 3b and S6. Peak deconvolution of H_2-TPR profiles revealed the presence of nano-Ga_2O_3, GaO^+, and EF-Ga_2O_3 on ZSM-5, modified-ZSM-5_{xM}, and beta and

Y-zeolite supports. The composition of each gallium oxide species (nano-Ga_2O_3, GaO^+, and EF-Ga_2O_3) was quantified by considering their corresponding peak area. In particular, the GaO^+ peak composition for modified-ZSM-5 catalysts increased with increasing ZSM-5 modification severity, except for the Ga/ZSM-$5_{1.0M}$ case. The higher percentage of GaO^+ in the peak for Ga(5%)/ZSM-$5_{0.8M}$ than for the other catalysts could result from more gallium oxide migrating into the modified-ZSM-5 channels coupled with strong interaction with support hydroxyl groups. On the other hand, the lack of a GaO^+ peak for Ga/ZSM-5 catalyst suggested that a negligible amount of gallium could migrate into zeolite channels where it could interact with hydroxyl groups. Thus, enhancing the mesopore volume of ZSM-5_{xM} supports promoted gallium oxide penetration into the pores, facilitated gallium oxide cationic species formation by strong interactions with the support hydroxyl groups, and the increased reduction of cationic species at higher temperature.[27,44,45] At the other extreme, the loss in support crystallinity for Ga(5 wt.%)/ZSM-$5_{1.0M}$ and disturbed the pore structure possibly caused a drop in metal-support interactions, with the result that the GaO^+ peak percentage was lower than for the Ga(5 wt.%)/ZSM-$5_{0.8M}$ catalyst.

Similarly, three gallium oxide reduction peaks corresponding to nano-Ga_2O_3, GaO^+, and EF-Ga_2O_3 were observed for 2, 5, and 8 wt% Ga loadings on ZSM-$5_{0.8M}$ catalysts. The nearly identical nano-Ga_2O_3 peak compositions (~10 %) for 5 and 8 wt% Ga loadings and higher (18%) values for 2 wt% Ga loading on ZSM-$5_{0.8M}$ suggested that lower Ga loadings facilitated enhanced Ga dispersion on external surface of the ZSM-$5_{0.8M}$ support, as evidenced in Table S4. Interestingly, the GaO^+ peak percentage increased from 37% to 54% when the Ga loading was increased from 2 to 5 wt% on ZSM-$5_{0.8M}$ support but then dropped to 33% when the Ga loading was raised to 8 wt% for the ZSM-$5_{0.8M}$ case.

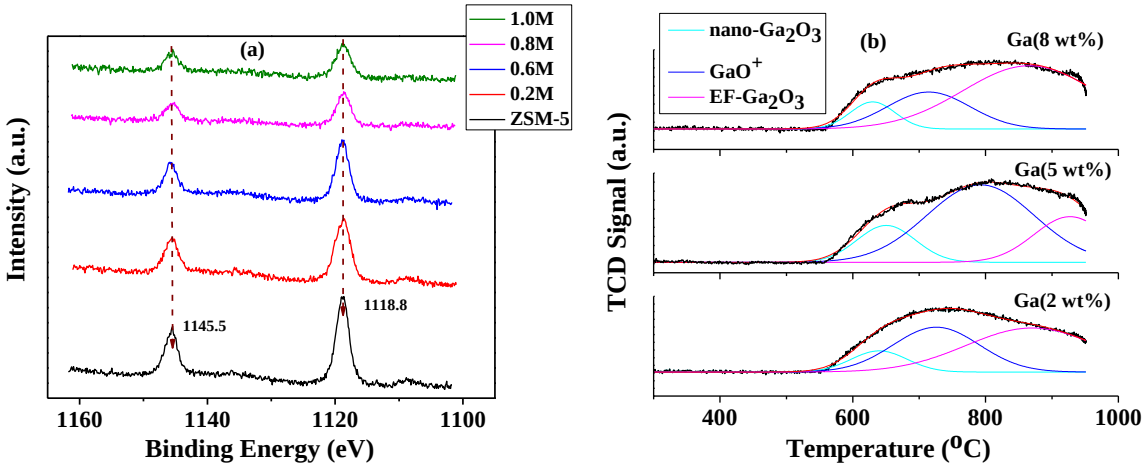

Figure 3: (a) XPS spectra of Ga(5 wt.%)/ZSM-5 and Ga(5 wt.%)/ZSM-5_{xM} catalysts in the binding energy range for the Ga 2p3/2 peak. (b) H_2-TPR profiles at selected loadings of Ga on ZSM-$5_{0.8M}$ catalysts.

In addition, the shift in GaO^+ peak position to higher temperature for 5 wt% Ga/ZSM-$5_{0.8M}$ compared to other formulations indicated more gallium oxide migrated into modified zeolite channels where it could interact strongly with hydroxyl groups inside the pores. The percentage of gallium oxide clusters (EF-Ga_2O_3) was higher in the peak for 8 wt% Ga/ZSM-$5_{0.8M}$ catalyst compared to lower loadings (2 and 5 wt%) of Ga on ZSM-$5_{0.8M}$. Thus, it became clear that the 5 wt% Ga loading was optimal for generating Ga_2O_3 nanoparticles and GaO^+ species while further increasing the Ga loading led to formation of gallium oxide clusters as EF-Ga_2O_3 particles.

Effect of catalyst modification on ethanol product distributions: Ethanol conversion to liquid, i.e., C5+, hydrocarbons is reported to occur via a dual-cycle hydrocarbon pool involving ethanol dehydration followed by aromatization. According to this mechanism, the ethanol hydrocarbon pool (HCP) reaction starts by producing ethylene that the inherent H-ZSM-5 pore structure converts to BTX.[14,23] During the ethanol HCP process, only a limited quantity of C9-C10 aromatic hydrocarbons can be formed due to their large size relative to the pore size/volume

capacity.[23] Thus, desilicating parent ZSM-5 (Si/Al = 23) by treating with different concentrations of NaOH removes framework silica to create mesopores that should be able to accommodate larger hydrocarbon molecules. As a result, the pore volume should be sufficient to accommodate more intermediate olefins and aromatics (BTX) for single stage conversion into C9-C10 aromatics. The larger pores in modified ZSM-5 supports should also increase LHYs by allowing a much greater fraction of active metal to impregnate inside the zeolite pores.

Alkali treatment of H-ZSM-5 is very selective for hydrolyzing the framework silica without disturbing framework alumina or Bronsted acid sites much.[30,33,47] But zeolite crystallinity can be damaged if alkali treatment extracts too much framework silica. Hence, ZSM-5 crystallinity and pore volume were characterized to determine how the concentration of NaOH impacted these properties and their relationship to carbon number distribution of product hydrocarbons. It was found that increasing NaOH concentration consistently increased support pore volume. However, treatment with 0.8M NaOH was optimum for generating mesopores in ZSM-$5_{0.8M}$ without compromising crystallinity as further increasing the alkali concentration to 1.0M NaOH resulted in excessive extraction of framework silica. The ICP-OES data in Table S1 shows this detrimental influence of 1.0M NaOH on ZSM-$5_{1.0M}$ crystallinity as measured by XRD. J. C. Groen et al found that alkali treatment of ZSM-35 that had a Si/Al ratio of 40 contained a high density of Si-O-Si bonds that are more easily hydrolyzed by NaOH, such that treatment with 0.2M NaOH at 60 °C for 30 minutes led to the maximum mesopore volume without disturbing zeolite crystallinity or Bronsted acidity. However, for the present study with a Si/Al ratio of 23 for parent ZSM-5, the greater proportion of more recalcitrant Si-O-Al bonds makes it necessary to apply higher concentrations of NaOH for hydrolysis than needed for less recalcitrant Si-O-Si bonds in the earlier report. Therefore, 0.8M NaOH treatment at 60°C for 30 minutes was required to dissolve

framework silica and to create mesopores without significantly disturbing crystallinity. Generally, because solvated Ga^{+3} ions for wet-impregnation are too large to enter ZSM-5 pores or exchange with Bronsted acid sites, they deposit as clusters on the external surface of the zeolite.[28,29,45,48] In line with this expectation, STEM showed large needle shape gallium oxide particles on the external surface of the parent H-ZSM-5 support in the present study. Interestingly, because the enhanced pore volume of H-ZSM-$5_{0.6,0.8\&1.0M}$ supports facilitated gallium oxide migration into zeolite channels, less gallium oxide was left on the external surface with the result that smaller gallium oxide particles were formed compared to parent ZSM-5. Calculating the Si/Ga ratio on the external surface based on XPS measurements reinforced that larger pores resulted in less Ga on the external surface of Ga(5 wt.%)/ZSM-$5_{0.6,0.8\ \&1.0M}$ compared to Ga(5 wt.%)/ZSM-5. Further, employing H_2-TPR revealed that enhancing pore volume resulted in more gallium migrating into the zeolite channels, thereby increasing GaO+ ions formation via interactions between gallium oxide and the modified-ZSM-5_{xM} supports.

The goal of this study was to maximize liquid product yields from ethanol through ZSM-5 modifications coupled with optimizing reaction temperature and WHSVs. Previous reports show that complete ethanol dehydration to form gas products (C1-C4 hydrocarbons) occurs at 200°C-300°C,[10–18] and ethanol aromatization to liquid products takes place above 350°C.[19–22,46,49] Hence, to increase liquid hydrocarbon formation, ethanol oligomerizations were conducted from 350°C to 500°C at different space velocities of 1.6, 0.8, and $0.4h^{-1.}$

Figure 4 shows the effect of temperature on ethanol liquid product distribution using Ga(5 wt.%)/ZSM-5 and Ga(5 wt.%)/ZSM-5_{xM} catalysts. All catalysts completely converted ethanol over a temperature range of 350°C to 500°C. The liquid hydrocarbon composition as analyzed by GC

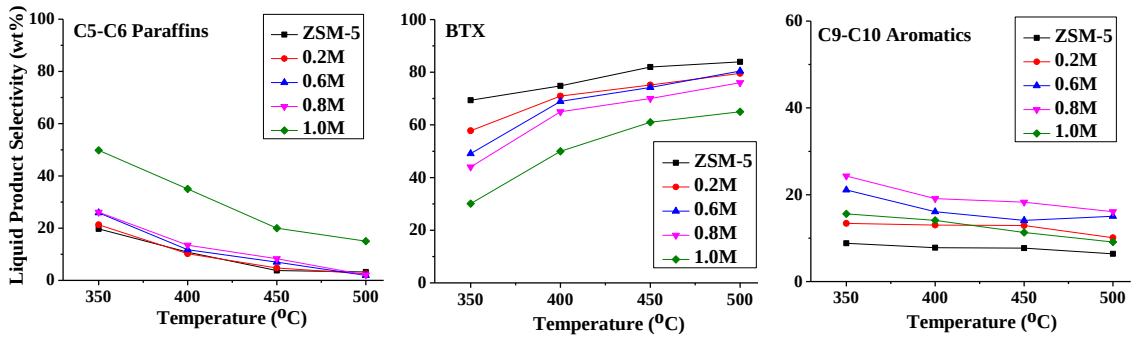

Figure 4: The effect of temperature on liquid product distribution from ethanol reactions on Ga(5 wt.%)/ZSM-5 and Ga(5 wt.%)/ZSM-5_{xM} catalysts at 1.6h^{-1} WHSV. Product selectivity is calculated based on the total mass of liquid hydrocarbons.

after separating the organic liquid from the aqueous phase was divided into C5-C6 paraffins, BTX, and C9-C10 aromatics [trimethyl benzene, ethyl methyl benzene and ethyl dimethyl benzene]. As shown in Figure 4 at 350°C, BTX selectivity in the liquid products dropped in the order of Ga-ZSM-5 (69.3%) > Ga/ZSM-$5_{0.2M}$ (57.8%) > Ga/ZSM-$5_{0.6M}$ (49.1%) > Ga/ZSM-$5_{0.8M}$ (44%) > Ga/ZSM-$5_{1.0M}$ (30.1%). On the other hand, this data show that C5-C6 paraffins selectivity in liquid products followed the opposite trend, with Ga/ZSM-$5_{1.0M}$ in particular realizing the highest C5-C6 paraffins selectivity compared to other catalysts. The C9-C10 aromatics selectivity in liquid products at 350°C dropped in the order Ga/ZSM-$5_{0.8M}$ (24.3%) > Ga/ZSM-$5_{0.6M}$ (21.1%) > Ga/ZSM-$5_{1.0M}$ (15.6%) > Ga/ZSM-$5_{0.2M}$ (13.4%) > Ga/ZSM-5 (8.1%). Thus, Ga/ZSM-$5_{0.8M}$ realized higher C9-C10 aromatics selectivity than the other catalysts and nearly three times as much as for the parent Ga/ZSM-5. This increase appears to be due to alkali treatment increasing pore volumes while preserving crystallinity as evidenced by lower C9-C10 aromatics and higher C5-C6 paraffins selectivities for ZSM-$5_{1.0M}$ with even greater pore volume but lower crystallinity.

Because the highest selectivity to C9-C10 chain lengths in liquid products was at 350°C, further experiments were conducted at this temperature for WHSVs of 0.4h^{-1} and from 0.8h^{-1} to 1.6h^{-1}.

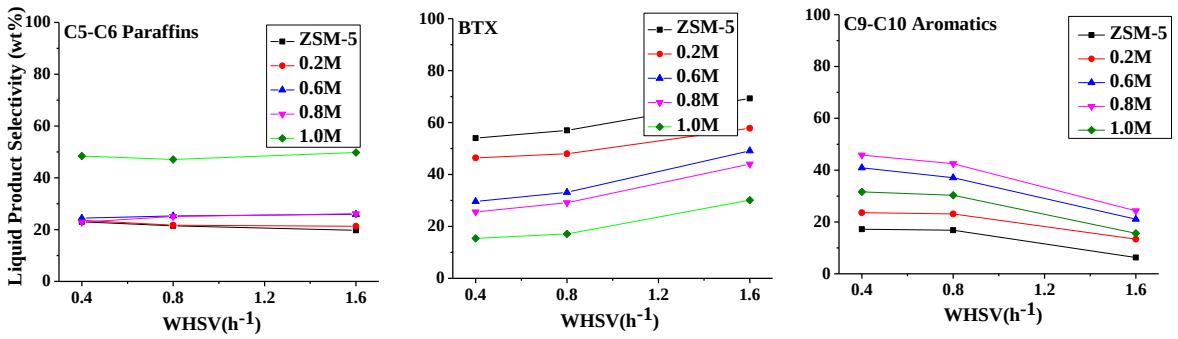

Figure 5: Effect of WHSVs on selectivities for formation of C5-C6 paraffins, BTX, and C9-C10 aromatics from reaction of ethanol over Ga(5 wt.%)/ZSM-5 and Ga(5 wt.%)/ZSM-5_{xM} catalysts at 350°C. Product selectivity is calculated based on the total mass of liquid hydrocarbons.

Figure 5 shows that these changes in WHSVs did not have much influence on C5-C6 paraffin selectivity for all catalysts and that Ga/ZSM-$5_{1.0M}$ catalyst still produced the highest selectivity to C5-C6 paraffins of nearly 50% for all WHSVs. However, BTX and C9-C10 aromatic selectivities changed with WHSVs. Interestingly, the lower 0.4 and 0.8h^{-1} WHSVs favored C9-C10 aromatics production at the expense of BTX. The selectivity of C9-C10 aromatics in liquid products increased nearly 3 times when the WHSV was dropped from 1.6h^{-1} (17.2% selectivity) to 0.4h^{-1} (6.3% selectivity) for the parent Ga/ZSM-5 catalyst. A minimal drop in C9-C10 aromatics selectivity resulted from increasing WHSVs from 0.4 to 0.8h^{-1} for all catalysts. Among the modified catalysts, Ga/ZSM-$5_{0.8M}$ had the highest selectivity to C9-C10 aromatics at 1.6h^{-1} (24.3%) and 0.4h^{-1} (45.8%) WHSVs.

To understand the effect of Ga loading coupled with alkali treatment on ethanol LHYs and product carbon number distribution, ethanol was reacted using bare ZSM-5 and ZSM-5_{xM} supports without loading gallium oxide at the previously optimized conditions of 350°C and 0.4h^{-1} WHSV. As shown in Figure 6(a), the extent of pore modification significantly increased LHYs with ZSM-$5_{0.8M}$ reaching 27.1% and ZSM-$5_{1.0M}$ increasing yields to 30.3%, the latter being nearly six times that from the 5.3% LHY from operation of the parent ZSM-5 support.

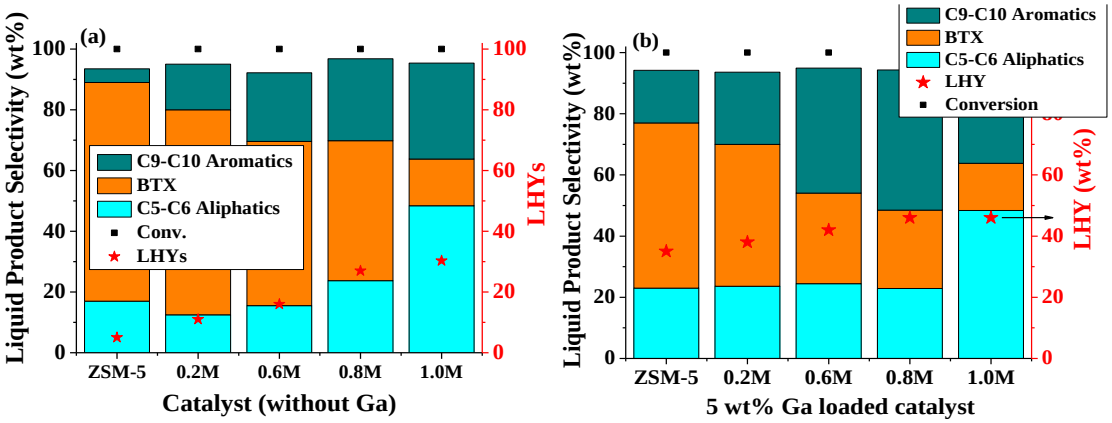

Figure 6: (a) Selectivity to C5-C6 paraffins, BTX, and C9-C10 aromatics produced by ethanol oligomerizations at 350°C and 0.4h^{-1} WHSV over ZSM-5 and ZSM-5_{xM} supports without loading Ga. (b) Selectivity to C5-C6 paraffins, BTX, and C9-C10 aromatics produced by ethanol oligomerizations over Ga(5 wt.%)/ZSM-5 and Ga(5 wt.%)/ZSM-5_{xM} at 350°C and 0.4h^{-1} WHSV. Product selectivity is based on the total mass of just liquid hydrocarbons.

As shown by comparing Table 1(pore volume data) and Figure 6(a), LHYs increased with increased newly generated pore volume of modified ZSM-5_{xM} supports. These results indicate that the enhanced pore volume accommodated more ethanol reactive intermediates inside the pores and promoted tandem dehydration-aromatization reactions. The 27.1% LHYs with 73.1% selectivity to aromatics (46.1% of BTX and 27% of C9-C10 aromatics) can be attributed to the combined contributions of enhanced pore volume and crystallinity for ZSM-$5_{0.8M}$. Although the LHYs achieved were greater from ZSM-$5_{1.0M}$ than from ZSM-$5_{0.8M}$, C5-C6 paraffins (selectivity 48.4%) were more prominent than BTX (15.4%) and C9-C10 aromatics (31.6%) in the liquid products. These results clearly suggest that ZSM-5 crystallinity is vital to producing higher molecular weight hydrocarbons, i.e., BTX and C9-C10 aromatics.

Comparing Figure 6a to Figure 6b shows that loading Ga onto ZSM-5 and modified-ZSM-5_{xM} significantly affected ethanol LHYs and C9-C10 aromatics selectivity by promoting the dual-cycle hydrocarbon pool path. In particular, loading 5 wt.% Ga onto ZSM-5, ZSM-$5_{0.6M}$, and ZSM-$5_{0.8M}$

resulted in 7, 2.6, and 1.7 times higher LHYs, respectively, compared to corresponding supports that were not loaded with Ga. Figure 7 shows that the incremental increase in C9-C10 aromatics selectivity correlated well with enhanced pore volume and increased surface Si/Ga ratios. The consistent increase in pore volume with increasing NaOH concentrations for treatment of ZSM-5 supports promoted more Ga migration into the modified-zeolite channels. Hence, the XPS measured surface Si/Ga ratios for both Ga(5 wt.%)/ZSM-$5_{0.8M}$ and Ga(5 wt.%)/ZSM-$5_{1.0M}$ catalysts are higher, suggesting that more Ga migrated into the larger modified zeolite channels. Enhancing Ga migration while retaining crystallinity in modified ZSM-5_{xM} supports enabled strong interactions between gallium oxide and the hydroxyl groups in ZSM-5_{xM} support, as shown by H_2-TPR. Specifically, H_2-TPR showed that increasing the percentage of GaO^+ species in modified zeolite channels promoted alkylation and hence, increased C9-C10 aromatics selectivity at the expense of BTX. On the other hand, the location of most of the Ga on the external surface of ZSM-5 only promoted dehydration and aromatization with the result that BTX was the major product. Combining greater gallium migration inside zeolite pores with enhanced metal-support interactions to form GaO^+ species for Ga(5 wt.%)/ZSM-$5_{0.8M}$ catalyst promoted the tandem reactions of ethanol dehydration, aromatization, and alkylation to increase LHYs and C9-C10 aromatics formation. Although the pore volume was greater for Ga(5 wt.%)/ZSM-$5_{1.0M}$, loss of support crystallinity and weak metal-support interactions (less percent of GaO^+ species) led to a drop in C9-C10 aromatic selectivity. Thus, the results shown in Figure 7 strongly suggest that the type of pore structure, greater ZSM-$5_{0.8M}$ pore volumes that accommodate longer chain lengths, and greater Ga penetration into the pores for Ga/ZSM-$5_{0.8M}$ catalyst combined with retained crystallinity and greater metal-support interactions significantly enhanced C9-C10 aromatics selectivity.

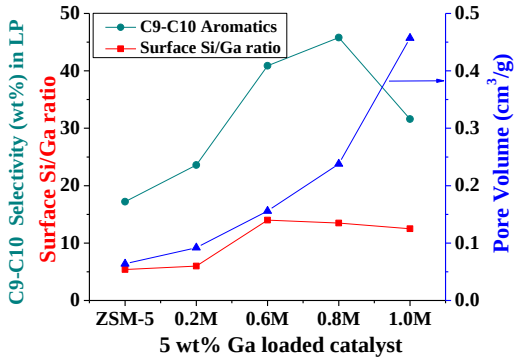

Figure 7: Correlation between C9-C10 aromatics selectivity and pore volume and surface Si/Ga ratios (LP: Liquid Product). Product selectivity is based on the total mass of liquid hydrocarbons produced.

Although TPR data for Ga(5%)/beta and Ga(5 wt%)/Y-zeolites revealed the presence of nano-Ga_2O_3, GaO^+ species, and Ga_2O_3 clusters, no liquid hydrocarbon products were formed from ethanol under similar reaction conditions of 350 °C and 0.4h^{-1} WHSV. Thus, it is clear that the combination of larger ZSM-5 pore structure with enhanced GaO^+ ions inside the ZSM-5 channels played important roles in increasing liquid product selectivity.

In order to evaluate the effect of catalyst synthesis time on Ga migration into ZSM-$5_{0.8M}$ channels, Ga wet-impregnation times of 4 hours and 32 hours were applied for production of two additional batches of Ga(5 wt.%)/ZSM-$5_{0.8M}$ catalysts. As XPS measurements show in Figure S5 and Table S3, the surface Si/Ga ratio for the 4 hour batch of Ga/ZSM-$5_{0.8M}$ catalyst was 9 while that for the 16 hours batch was measured to be about two thirds of that value. These results indicate that more Ga was deposited on the external surface of the zeolite that had been synthesized for 4 hours while impregnating for 16 hours allowed more Ga to migrate into the pores, a conclusion that is also supported by the bulk elemental analysis reported in Table S2. Furthermore, because the surface Si/Ga ratio was the same for catalysts that were synthesized for 16 and 32 hours, a 16 hour impregnation was adequate to maximize Ga insertion into ZSM-$5_{0.8M}$ channels. When Ga(5

wt.%)/ZSM-$5_{0.8M}$ catalysts that had been impregnated for 4 hours, 16 hours, and 32 hours were employed for ethanol conversion to hydrocarbons at 350°C and 0.4h^{-1} WHSV, Figure 8(a) shows that C9-C10 aromatics selectivity in the liquid products increased from 20.1% for the 4 hours synthesis time to 45.6% for a 16 hours synthesis and then changed little to 43.9% for a 32 hour time. These results clearly reveal that the high fraction of Ga inside the zeolite channels not only facilitated ethanol dehydration and aromatization but also promoted alkylation to higher C9-C10 aromatics selectivity while alkylation was impeded when less Ga was inside the pores.

The effect of Ga on hydrocarbon product distribution was evaluated by loading 2 wt.% and 8 wt.% Ga on ZSM-$5_{0.8M}$ while keeping the catalyst synthesis time at 16 hours. Figure 8(b) shows that compared to results for 5 wt.% Ga, 2 wt.% and 8 wt.% Ga loadings produced more C5-C6 paraffins and BTX, respectively, while suppressing C9-C10 aromatics formation. In the case of 2 wt.% Ga/ZSM-$5_{0.8M}$, the lower loading of gallium oxide suppressed aromatization and resulted in more C5-C6 paraffins. On the other hand, the 8% Ga loading have blocked zeolite pores and interfered with escape of C9-C10 aromatics from the pores due to steric constraints, as supported by the N_2-physisorption results shown in Figure S2.

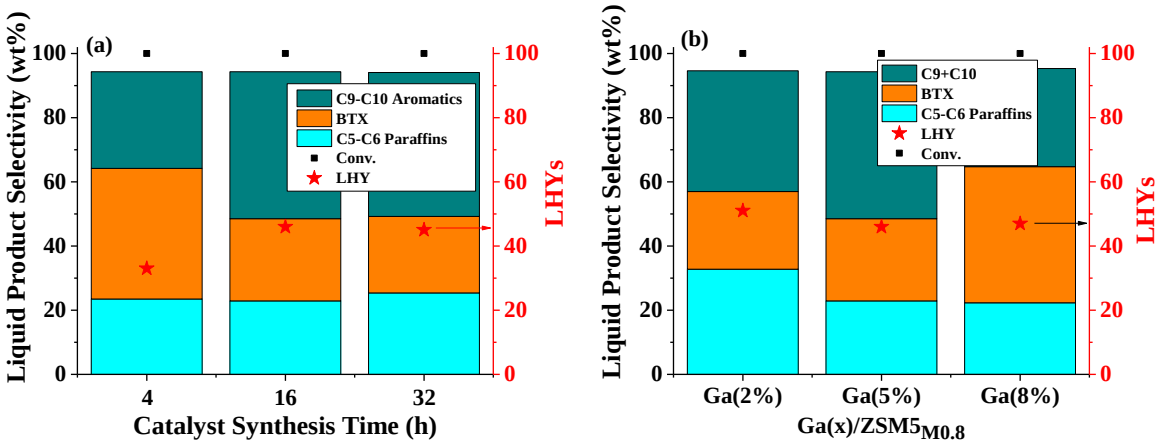

Figure 8: Effect of (a) catalyst synthesis time and (b) Ga content on liquid hydrocarbon product selectivity following reaction of ethanol on Ga(5 wt.%)/ZSM-$5_{0.8M}$ catalysts at 350°C with a 0.4h^{-1} WHSV. Product selectivity is based on total liquid hydrocarbons.

The result that the surface Si/Ga ratios of 5 wt.% Ga/ZSM-$5_{0.8M}$ and 8 wt.% Ga/ZSM-$5_{0.8M}$ catalysts as measured by XPS had about the same values suggests that migration of more gallium oxide into zeolite channels for the latter case reduced formation of larger chains by blocking pores. Although the surface Si/Ga ratio of 29 for 2 wt.% Ga/ZSM-$5_{0.8M}$ meant more Ga was in the pores, the lower amount of Ga left to enter the zeolite channels than for 5 wt.% loadings would be expected to reduce C9-C10 aromatics yields.

Figure 9a shows that ethanol LHYs and >45% C9-C10 aromatics selectivities were maintained for 32 hours for the Ga(5 wt.%)/ZSM-$5_{0.8M}$ catalyst. Thus, it appears that enhanced zeolite pore volume and Ga metal insertion into ZSM-$5_{0.8M}$ channels maintained catalyst activity over these time periods without loss of C9-C10 aromatics selectivity. Ga(5 wt.%)/ZSM-$5_{0.8M}$ stability was also evaluated when fed wet-ethanol vapor (40% vol), about the concentration that would be produced by vaporizing fermentation broth at the feed tray to an ethanol recovery distillation train.[4] As shown in Figure 9b, LHYs and C9-C10 aromatics selectivity were both higher when Ga(5 wt.%)/ZSM-$5_{0.8M}$ was fed wet ethanol at 350°C with a $0.4h^{-1}$ WHSV than when just pure ethanol was the feed at the same conditions. Furthermore, the C9-C10 aromatics selectivity drifted upward to 55.1% at 20 hours reaction time for wet ethanol and then remained about the same after that. Previous reports that steam treatment of ZSM-5 can increase catalyst stability and affect final product distributions by facilitating new mesopores formation could account for greater C9-C10 aromatics selectivity in the present case.[50]

Hence, to determine the change in physical and chemical properties of catalysts used to convert pure ethanol and wet ethanol to hydrocarbons and the influence of water on C9-C10 aromatic selectivity, used catalysts were extensively characterized by XRD, N_2-physisorption, H_2-TPR, and TPO.

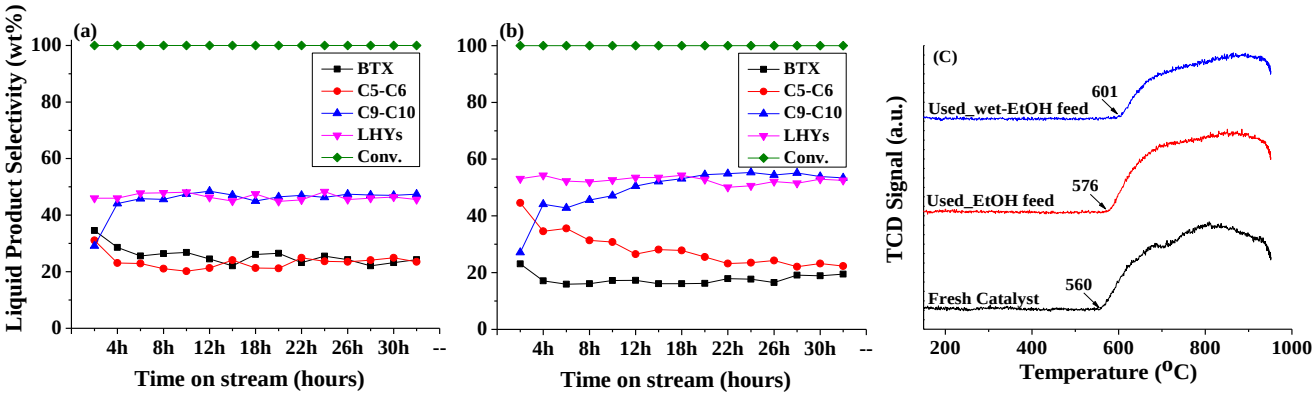

Figure 9: (a) Product selectivity over time for Ga/ZSM-$5_{0.8M}$ fed ethanol for 32 hours and (b) product selectivity over time for Ga/ZSM-$5_{0.8M}$ fed wet-ethanol for 32 hours at 350°C and 0.4h^{-1} WHSV. Product selectivity is based on total liquid hydrocarbons. (c) H_2-TPR profiles of fresh catalyst and used catalysts for ethanol and wet-ethanol stream.

As shown in Figure S9, XRD revealed that the support crystallinity did not change after several hours of reactions with pure of wet ethanol, indicating the zeolite framework was not damaged at longer times. However, the top layer of used catalysts turned dark black while the gray color of the middle and lower portions suggested carbon formation progressed slowly through the catalyst.

Figure S10 indicates a marginal loss in total surface area for used catalysts due to partial damage to the micropore surface area of the ZSM-$5_{0.8M}$ support. A marginal loss in mesopore volume was observed for used catalysts compared to fresh catalyst and the pore volume dropped in order of Ga/ZSM-$5_{0.8M}$ (0.2483 cm^3/g; fresh catalyst) > used Ga/ZSM-$5_{0.8M}$ for wet-ethanol feed (0.2279 cm^3/g) > used Ga/ZSM-$5_{0.8M}$ for ethanol feed (0.2164 cm^3/g). The loss in pore volume for used Ga/ZSM-$5_{0.8M}$ catalysts cause either pore blocking by extra framework alumina (EFAl) species which are leached out from zeolite framework or migration of more gallium from the surface into the mesopores for ethanol conversion at 350 °C.

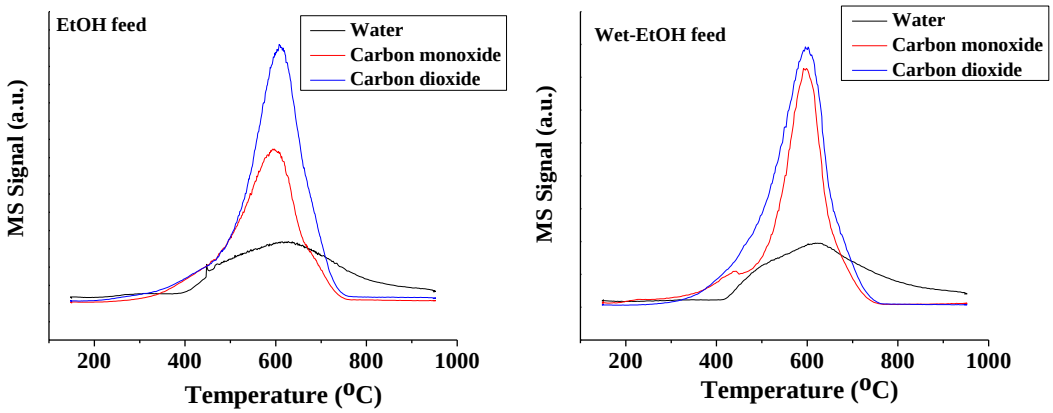

Figure 10: TPO profiles of catalysts following their use for conversion of pure ethanol and wet-ethanol to hydrocarbons.

Interestingly, the shift of the H_2-TPR profiles of gallium oxide reduction peaks to higher temperatures shown in Figure 9c for used catalysts compared to fresh Ga/ZSM-$5_{0.8M}$ catalyst suggests enhanced interactions between gallium oxide and support hydroxyl groups that occurred during ethanol and wet-ethanol conversions. In particular, catalyst used with wet-ethanol showed gallium oxide reduction starting from 601°C, a higher temperature than for catalyst used with pure ethanol (576°C) and fresh catalyst (560°C). These results suggest that more gallium migrated into the zeolite pores and enabled strong metal-support interactions, resulting in higher C9-C10 aromatic selectivity. TPO experiments were conducted to determine the extent of formation of soft carbon (hydrogen rich hydrocarbons) versus hard carbon (hydrogen lean polyaromatics or graphite type carbon) on used catalysts.[46] Figure 10 shows desorption peaks for carbon dioxide, carbon monoxide, and water produced by burning off the carbon from used catalysts. The high coke combustion temperatures suggest that a substantial amount of hard carbon had been formed on the catalysts, likely via polymerization of aromatic compounds during conversion of both pure and wet ethanol. However, the amount of carbon produced was lower from used catalyst that had been used with wet (4.8 wt.%) than with pure ethanol (7.1 wt.%).

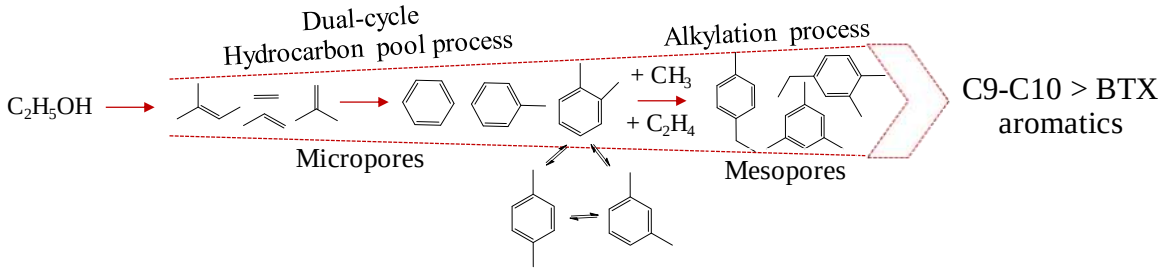

Scheme 1: Progressive increase in carbon number as ethanol dehydrates, aromatizes, and alkylates to longer chained hydrocarbons and C9-C10 aromatics along H-ZSM-5 meso-micropores before exiting through large pores through which they can fit. If the hydrocarbon grows to a size that is too large to exit, it must either crack to form smaller molecules that can leave or pyrolyze to form carbon deposits that block access to active sites or restrict hydrocarbons from entering or leaving pores.

Previous studies showed less than 5% C9+ aromatics formation in addition to light weight hydrocarbons and BTX from an ethanol feed.[22,23] The high molecular weight C9+ hydrocarbon may occur either on the external ZSM-5 surface or inside its pores by alkylation of C7/C8 aromatics with C1/C2 paraffin. Any chains too long to escape through the pore mouth would need to either crack to smaller molecules that could leave through zeolite micropores or breakdown to deposit carbon on the walls that would interfere with adsorption or block micropores. However, this study showed the catalyst could maintain stable production of C9-C10 aromatics, mostly as ethyl methyl benzene, trimethyl benzene (mesitylene), and ethyl dimethyl benzene (C10). As illustrated in Scheme 1, the combination of micro and mesopores in modified-ZSM-5 supports could accommodate sequential ethanol dehydration, aromatization, and alkylation and reduce trapping of bulky C9-C10 aromatics that would otherwise either crack to smaller molecules that could escape or pyrolyze to coke that would interfere with catalytic activity inside the pores.

The present study provides insights into the roles of zeolite pore volume, crystallinity, and gallium penetration into channels and metal-support interactions on the distribution of hydrocarbon chain lengths produced by reaction of ethanol to liquid hydrocarbons on ZSM-5

catalysts. Although ZSM-5 alone produced aromatic hydrocarbons, LHYs were very low due to support micro porosity. Treatment of ZSM-5 with 1.0M NaOH increased pore volume, but selectivity to liquid hydrocarbons containing more than 5 carbon atoms (C6+) dropped significantly due to loss of support crystallinity and metal-support interaction. However, by maintaining crystallinity while also increasing pore volume, treatment of ZSM-5 with 0.8M NaOH increased both LHYs and selectivity to C6+ hydrocarbons. Furthermore, enlarging pores by treatment with NaOH increased C9-C10 selectivity by nearly 50% from ethanol dehydration, aromatization, and alkylation through promoting gallium migration into ZSM-$5_{0.8M}$ channels and enabling strong metal-support interactions. Finally, the ZSM-5 inherent pore structure played a key role in controlling LHYs compared to other large pore zeolites (Figure S12).

Conclusions

This study reveals how pore modification, crystallinity, Ga proximity and metal-support interactions in zeolite channels affect yields and carbon number distributions of hydrocarbons formed by single step reaction of ethanol on ZSM-5 catalysts. Treatment of ZSM-5 with 0.2, 0.6, 0.8, and 1.0M NaOH progressively increased pore volume/size, but crystallinity dropped significantly for 1.0M NaOH as determined by XRD and N_2-physisorption studies. In addition, STEM and XPS studies revealed greater Ga migration into the channels of ZSM-5 that had been treated with 0.8 and 1.0M NaOH than for parent ZSM-5 catalyst. H_2-TPR studies revealed that enhanced gallium migration into the mesopores further promoted GaO^+ ions formation via strong metal support interactions. The ability of ZSM-5 catalysts treated with 0.8M NaOH but without gallium oxide to accommodate larger hydrocarbon molecules in the larger pores combined with retained crystallinity and greater Ga penetration followed by GaO^+ ions formation into zeolite pores increased LHYs yields by nearly five times to 27.1% compared to 5.3% from the parent

support. Loading ZSM-$5_{0.8M}$ with 5 wt.% Ga further increased LHYs to 46.1% and C9-C10 hydrocarbon selectivity to 45.8% from 35.1% and 17.2%, respectively, for reaction with the parent catalyst at 350°C and $0.4h^{-1}$ WHSV. Furthermore, feeding 40% ethanol in water vapor increased LHYs to ≥50% and C9-C10 aromatic selectivity to 55.1% while maintaining catalyst stability over 32 hours.

Acknowledgements

Funding for this research was provided by The Center for Bioenergy Innovation, a U.S. Department of Energy Research Center supported by the Office of Biological and Environmental Research in the DOE Office of Science. The authors appreciate assistance by Dr. Krassimir N. Bozhilov with use of the electron microscope at the Central Facility for Advanced Microscopy and Microanalysis (CFAMM) at the University of California Riverside. Dr. Ilkeun Lee provided valuable assistance with XPS analysis that was made possible by NSF grant DMR-0958796. The authors also thank Brent Scheidemantle and Dr. Charles M Cai for construction of the fixed-bed reactor used for these experiments. Dr. Kandis Leslie Gilliard-Abdulaziz at the University of California Riverside provided access to the H_2-TPR and TPO instruments used for this study and Mr. Soham Shah and Mr. Somchate Wasantwisut of her team helped in these experiments. Authors also thank Dr. Aibolat Koishyb and Dr. Zhenglong Li for assistance in obtaining NH_3-TPD data. The authors also thank Professor Phillip Christopher and Justin Marlowe at the University of California Santa Barbara for obtaining temperature program desorption data.

Conflict of interest. Dr. Bhogeswararao Seemala has no conflicts to declare. Dr. Charles Wyman is a cofounder and president and CEO of Vertimass LLC. Vertimass is working to commercialize zeolite catalysts for conversion of ethanol into hydrocarbons. Dr. Charles E. Wyman is also the founding Editor-in-Chief of the journal *Biotechnology for Biofuels*.

References:

1 U.S. Energy Information Administration (EIA), *https://www.eia.gov/environment/emissions/carbon/pdf/2019_co2analysis.pdf*.

2 EPA, *Invent. U.S. Greenh. Gas Emiss. Sink.*, 2019, **EPA430-R-2**, 2–99.

3 C. Yang and S. Yeh, *AIP Conf. Proc.*, 2011, **1401**, 259–270.

4 J. R. Hannon, L. R. Lynd, O. Andrade, P. T. Benavides, G. T. Beckham, M. J. Biddy, N. Brown, M. F. Chagas, B. H. Davison, T. Foust, T. L. Junqueira, M. S. Laser, Z. Li, T. Richard, L. Tao, G. A. Tuskan, M. Wang, J. Woods and C. E. Wyman, *Proc. Natl. Acad. Sci. U. S. A.*, 2020, **117**, 12576–12583.

5 J. Holladay, Z. Abdullah and J. Heyne, *Rev. Tech. Pathways*, 2020, 1–81.

6 C. Gutiérrez-Antonio, F. I. Gómez-Castro, J. A. de Lira-Flores and S. Hernández, *Renew. Sustain. Energy Rev.*, 2017, **79**, 709–729.

7 S. S. Doliente, A. Narayan, J. F. D. Tapia, N. J. Samsatli, Y. Zhao and S. Samsatli, *Front. Energy Res.*, 2020, **8**, 1–38.

8 J. Teter, P. Le Feuvre, P. Bains and L. Lo Re, *IEA, Paris*, 2020, https://www.iea.org/reports/aviation-2.

9 O. Rosales-Calderon and V. Arantes, *Biotechnol. Biofuels*, 2019, **12**, 2-58.

10 J. Bi, X. Guo, M. Liu and X. Wang, *Catal. Today*, 2010, **149**, 143–147.

11 N. Zhan, Y. Hu, H. Li, D. Yu, Y. Han and H. Huang, *Catal. Commun.*, 2010, **11**, 633–637.

12 Q. Sheng, K. Ling, Z. Li and L. Zhao, *Fuel Process. Technol.*, 2013, **110**, 73–78.

13 R. Barthos, A. Sze and F. Solymosi, *J. Phys. Chem. B*, 2006, **110**, 21816–21825.

14 K. K. Ramasamy and Y. Wang, *Catal. Today*, 2014, **237**, 89–99.

15 N. Viswanadham, S. K. Saxena, J. Kumar, P. Sreenivasulu and D. Nandan, *Fuel*, 2012,

95, 298–304.

16 K. Murata, M. Inaba and I. Takahara, *J. Japan Pet. Inst.*, 2008, **51**, 234–239.

17 S. Moon, H. J. Chae and M. B. Park, *Catalysts*, 2019, **9**, 1–12.

18 Z. Wang, L. A. O'Dell, X. Zeng, C. Liu, S. Zhao, W. Zhang, M. Gaborieau, Y. Jiang and J. Huang, *Angew. Chemie*, 2019, **131**, 18229–18236.

19 M. Inaba, K. Murata, M. Saito and I. Takahara, *React. Kinet. Catal. Lett.*, 2006, **88**, 135–142.

20 S. K. Saha and S. Sivasanker, *Catal. Letters*, 1992, **15**, 413–418.

21 K. Van Der Borght, V. V. Galvita and G. B. Marin, *Appl. Catal. A Gen.*, 2015, **504**, 621–630.

22 Z. Li, A. W. Lepore, M. F. Salazar, G. S. Foo, B. H. Davison, Z. Wu and C. K. Narula, *Green Chem.*, 2017, **19**, 4344–4352.

23 R. Johansson, S. L. Hruby, J. Rass-Hansen and C. H. Christensen, *Catal. Letters*, 2009, **127**, 1–6.

24 J. Jae, G. A. Tompsett, A. J. Foster, K. D. Hammond, S. M. Auerbach, R. F. Lobo and G. W. Huber, *J. Catal.*, 2011, **279**, 257–268.

25 P. Gallezot, C. Leclercq, M. Guisnet and P. Magnoux, *J. Catal.*, 1988, **114**, 100–111.

26 R. A. Van Santen and W. M. H. Sachtler, *J. Phys. Chem. B*, 1999, **103**, 4611–4622.

27 K. M. Dooley, C. Chang and G. L. Price, *Appl. Catal. A Gen.*, 1992, **84**, 17–30.

28 G. L. Price and V. Kanazirev, *J. Catal.*, 1990, **278**, 267–278.

29 A. Biscardi and E. Iglesia, *Catal. Today*, 1996, **31**, 207–231.

30 J. C. Groen, J. A. Moulijn and J. Pérez-Ramírez, *J. Mater. Chem.*, 2006, **16**, 2121–2131.

31 A. Čižmek, B. Subotić, I. Šmit, A. Tonejc, R. Aiello, F. Crea and A. Nastro, *Microporous*

Mater., 1997, **8**, 159–169.

32 K. Sadowska, K. Góra-Marek, M. Drozdek, P. Kuśtrowski, J. Datka, J. Martinez Triguero and F. Rey, *Microporous Mesoporous Mater.*, 2013, **168**, 195–205.

33 A. Aloise, A. Marino, F. Dalena, G. Giorgianni, M. Migliori, L. Frusteri, C. Cannilla, G. Bonura, F. Frusteri and G. Giordano, *Microporous Mesoporous Mater.*, 2020, **302**, 110198 (1–8).

34 R. M. Dessau, E. W. Valyocsik and N. H. Goeke, *ZEOLITES*, 1992, **12**, 776–779.

35 T. Suzuki and T. Okuhara, *Microporous Mesoporous Mater.*, 2001, **43**, 83–89.

36 R. Fricke, H. Kosslick and M. Richter, *Chem. Rev.*, 2000, **100**, 2303−2405.

37 L. I. U. Ru-ling, Z. H. U. Hua-qing, W. U. Zhi-wei, Q. I. N. Zhang-feng, F. Wei-bin and W. Jian-guo, *J. Fuel Chem. Technol.*, 2015, **43**, 961–969.

38 I. Nowak, J. Quartararo, E. G. Derouane and J. C. Védrine, *Appl. Catal. A Gen.*, 2003, **251**, 107–120.

39 H. Xiao, J. Zhang, X. Wang, Q. Zhang, H. Xie, Y. Han and Y. Tan, *Catal. Sci. Technol.*, 2015, **5**, 4081–4090.

40 E. S. Shpiro, D. P. Shevchenko, O. P. Tkachenko and R. V. Dmitriev, *Appl. Catal. A, Gen.*, 1994, **107**, 147–164.

41 A. Wang, D. Austin, H. Qian, H. Zeng and H. Song, *ACS Sustain. Chem. Eng.*, 2018, **6**, 8891–8903.

42 A. Wang, D. Austin, A. Karmakar, G. M. Bernard, V. K. Michaelis, M. M. Yung, H. Zeng and H. Song, *ACS Catal.*, 2017, **7**, 3681–3692.

43 K. Van Der Borght, V. V. Galvita and G. B. Marin, *Appl. Catal. A Gen.*, 2015, **492**, 117–126.

44 N. Al-Yassir, M. N. Akhtar, K. Ogunronbi and S. Al-Khattaf, *J. Mol. Catal. A Chem.*, 2012, **360**, 1–15.

45 R. Fricke, H. Kosslick, G. Lischke and M. Richter, *Chem. Rev.*, 2000, **100**, 2303–2405.

46 P. C. Lai, C. H. Chen, H. Y. Hsu, C. H. Lee and Y. C. Lin, *RSC Adv.*, 2016, **6**, 67361–67371.

47 J. Li, M. Liu, X. Guo, S. Zeng, S. Xu, Y. Wei, Z. Liu and C. Song, *Ind. Eng. Chem. Res.*, 2018, **57**, 15375–15384.

48 K. M. Dooley, G. L. Price, V. I. Kanazirev and V. I. Hart, *Catal. Today*, 1996, **31**, 305–315.

49 M. Seifert, M. S. Marschall, T. Gille, C. Jonscher, O. Busse, S. Paasch, E. Brunner, W. Reschetilowski and J. J. Weigand, *ChemCatChem*, 2020, **12**, 6301–6310.

50 Q. Sheng, K. Ling, Z. Li and L. Zhao, *Fuel Process. Technol.*, 2013, **110**, 73–78.